

Hydrodynamics and Mass Transfer of Gas–Liquid Flow in a Falling Film Microreactor

Haocui Zhang

Dalian Institute of Chemical Physics, Chinese Academy of Sciences, Dalian 116023, China
Graduate University, Chinese Academy of Sciences, Beijing 100049, China

Guangwen Chen, Jun Yue, and Quan Yuan

Dalian Institute of Chemical Physics, Chinese Academy of Sciences, Dalian 116023, China

DOI 10.1002/aic.11743

Published online April 7, 2009 in Wiley InterScience (www.interscience.wiley.com).

In this article, flow pattern of liquid film and flooding phenomena of a falling film microreactor (FFMR) were investigated using high-speed CCD camera. Three flow regimes were identified as “corner rivulet flow,” “falling film flow with dry patches,” and “complete falling film flow” when liquid flow rate increased gradually. Besides liquid film flow in microchannels, a flooding presented as the flow of liquid along the side wall of gas chamber in FFMR was found at high liquid flow rate. Moreover, the flooding could be initiated at lower flow rate with the reduction of the depth of the gas chamber. CO₂ absorption was then investigated under the complete falling flow regime in FFMR, where the effects of liquid viscosity and surface tension on mass transfer were demonstrated. The experimental results indicate that k_L is in the range of 5.83 to $13.4 \times 10^{-5} \text{ m s}^{-1}$ and an empirical correlation was proposed to predict k_L in FFMR.

© 2009 American Institute of Chemical Engineers *AICHE J.*, 55: 1110–1120, 2009

Keywords: microchannel, falling film, gas–liquid two-phase flow, mass transfer

Introduction

Falling film reactors were widely used for gas–liquid absorption and reaction process such as sulfonation, chlorination, ethoxylation, and hydrogenation.^{1,2} The main characteristic of this kind of reactor is the motion of a liquid film over a wetted surface under the effect of gravity. Such falling film reactor offers two main advantages including high capacity of mass transfer and low pressure drop in the reactor.

During recent years, microstructured reactors have gained increasing importance as useful devices for chemical processing such as gas–solid catalytic reactions,^{3–5} gas–liquid and liquid–liquid processes^{6–9} primarily because of their high rate of mass and heat transfer. A falling film microreactor

(FFMR) developed by Institut für Mikrotechnik Mainz¹⁰ was able to prevent break-up of the liquid film at very low flow rates and any phase intermixing.¹¹ Yeong et al.¹² investigated nitrobenzene hydrogenation over palladium catalyst in this type of FFMR and estimated volumetric mass transfer coefficient of hydrogen in liquid film qualitatively to be in the range of 3–8 s⁻¹ according to two-film theory, which is much higher than that obtained in traditional falling film reactors. However, mass transfer details in FFMR were not discussed in depth. Zanfir et al.¹³ developed a two-dimensional model to simulate CO₂ absorption in NaOH solution in FFMR and found that mass transfer in liquid side was the limiting step. This model was proposed under the assumption that the flow of falling film was continuous with a flat profile. In fact, liquid film profile in FFMR is usually curved instead of being completely flat. For example, Yeong et al.¹⁴ found that a flowing meniscus in microchannels existed under a wide range of flow rates by using laser scanning confocal microscopy. They also pointed out that it was

Correspondence concerning this article should be addressed to G. W. Chen at gwchen@dicp.ac.cn

difficult to measure exactly the thickness of liquid film at very low flow rates due to the limits of the instruments. In this case, the liquid film may be unable to completely cover the bottom wall of the microchannel.¹⁵ For industrial application, a large FFMR and a cylindrical one were designed by increasing the structured surface area to obtain higher pilot throughput. However, there was no precise match for better understanding of the reaction in them.¹⁶ Toward solving this problem, Al-Rawashdeh et al.¹¹ have recently proposed a pseudo 3D model based on realistic microchannel and film profile in FFMRs to simulate the liquid menisci, flow velocity, species transport, and reaction. Therefore, it is obvious that hydrodynamics of liquid film and mass transfer characteristics in FFMR still need to be further investigated. In this work, flow pattern of liquid film in FFMR has been observed by the use of a high-speed CCD camera. Then, CO₂ absorption in falling film of several liquids was used to evaluate the potential applications of FFMR. The dependence of CO₂ absorption rate on the operational condition, the physical properties of the liquid (such as density, viscosity, and surface tension), and channel surface properties were investigated.

Experimental Section

Reactor design

Figure 1 shows the design of FFMR used. It consists of plate A and B. Twenty straight open microchannels (1000 μm wide, 300 μm deep, and 60 mm long) were fabricated on plate A and a gas chamber located on plate B. Three FFMRs (FFMR I-III) were tested, where plate A remained unchanged and plate B with different depth of the gas chamber (d_G) was used. That is, d_G was fixed at 0.8, 1.45, and 3.0 mm for FFMR I, FFMR II, and FFMR III, respectively. All reactors were fabricated on the polymethyl methacrylate (PMMA) substrate by using precision milling technology. The value of surface roughness (Ra) of the microchannels measured by step profiler (ET4000M) is less than 0.30 μm and a typical channel profile can be found in the article of Zhao et al.⁸

To ensure uniform liquid flow in each FFMR, a rectangular horizontal header with cross-section of 3 mm \times 3 mm was fabricated on plate A, which was thereby fed to open microchannels. These microchannels were then connected with a collector which has the same structure to the inlet header in order to withdraw the liquid out of the reactor. When the two plates of A and B were pressed together, two small sections near the entrance and the exit of these microchannels (about 0.85 mm long) were covered by the top plate and the remaining section was in contact with the gas chamber serving as the gas-liquid contact zone.

The majority of the present experiments were performed in the nonmodified microchannels of FFMR (i.e., PMMA substrate). Only in the case concerning the effect of wettability on mass transfer in FFMR, these microchannels were modified in the following way to improve the wettability. First, plate A was washed by the ultrasonic vibration for 15 min, followed by drying under flowing air atmosphere. Then, the plate was coated with 1.0 mol l⁻¹ aluminum hydroxide sol by using a cleaned brush and dried under flowing air atmosphere again. The obtained layer is very thin (ca. 1.0

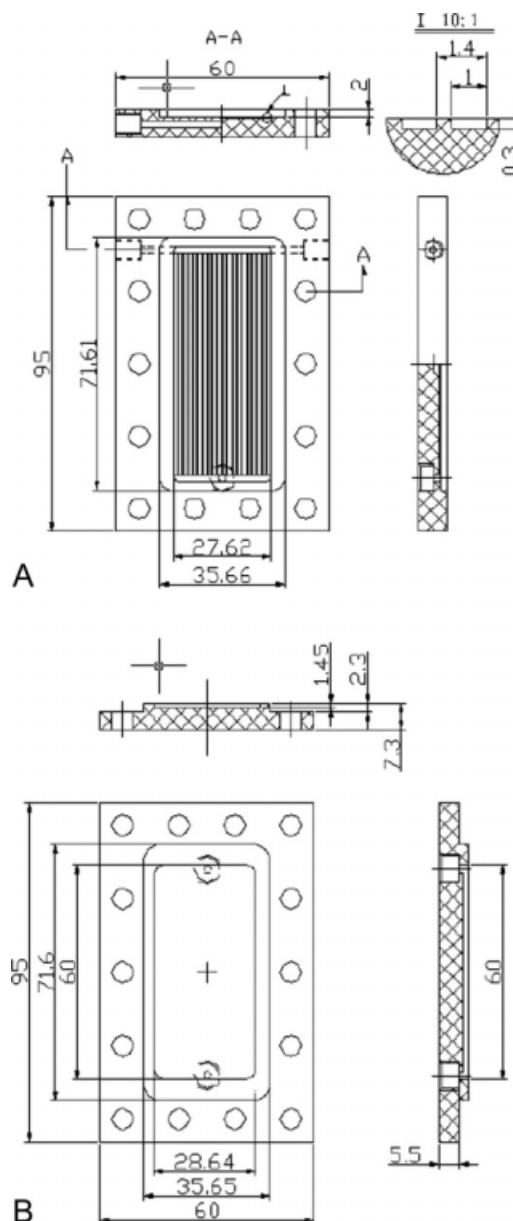


Figure 1. Two-dimensional drawing of FFMR (scale in mm).

μm), so that the size of cross section was not changed by this coating procedure.

Experimental setup

In this work, hydrodynamics of liquid film and gas-liquid mass transfer characteristics have been investigated in FFMR. The detailed experimental setup is shown in Figure 2. The liquid used was deionized water, 5.2 and 12 wt % ethylene glycol (EG) solutions, 50 and 110 ppm sodium laurylsulfate (SLS) solutions, whose physical properties are listed in Table 1 according to the data of references.^{17,18}

To generate a stable gas-liquid contacting pattern inside FFMR, the reactor was firstly filled with the liquid pumped from the reservoir. Then, the liquid and gas outlets were

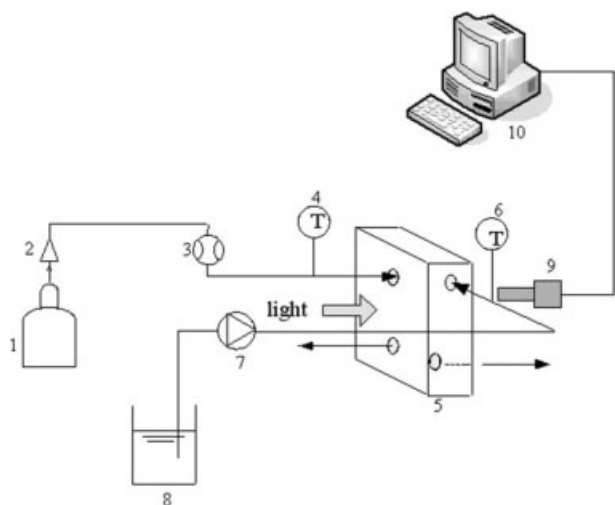


Figure 2. Schematic diagram of the absorption apparatus.

1: CO₂ cylinder; 2: pressure regulating valve; 3: gas mass flow controller; 4, 6: thermometer; 5: falling film microreactor; 7: pump; 8: reservoir; 9: CCD camera; 10: computer.

opened orderly so that the excessive liquid could be removed and a stable liquid falling film was formed in microchannels. CO₂ from the gas cylinder was regulated via a gas mass flow controller and flowed cocurrently into the gas chamber of the reactor. During the operations, gas bubbles may be accumulated in the horizontal header, which would cause nonuniform liquid flow among microchannels.¹⁹ When this occurred, the valve at the end of the header channel should be opened to let the flowing liquid drive the bubble out. Comparing with microchannels, the volume of the header channel is large enough so that a nearly uniform liquid flow distribution can be obtained.²⁰ The flow of liquid film was steady once formed. In the range of flow rates studied, gas and liquid can be separated completely. All experiments were performed under room temperatures (23–25°C). The flow rate of liquid ranged from 2 to 40 ml min⁻¹ and the flow rate of gas was fixed at 46 and 183 ml min⁻¹, respectively.

To observe flow pattern of liquid film in FFMR, a high-speed CCD camera was used. A cold lamp was used to provide a background illumination. The captured frames were then immediately transferred to the computer via a data acquisition system for further analysis.

In mass transfer experiments, liquid sample was collected in a beaker containing 30 ml NaOH (0.1 mol l⁻¹) and the

collecting time was recorded exactly. When the liquid entered into the beaker, CO₂ absorbed was converted to Na₂CO₃. Then, CO₂ concentration in the liquid flowing out of FFMR, C_{out} , can be derived from titration analysis of the mixture in the beaker using HCl solution with phenolphthalein and methyl orange as indicators for the corresponding endpoints, as Eq. 1 suggests

$$C_{out} = \frac{V_{HCl}C_{HCl}}{Q_L t} \quad (1)$$

where V_{HCl} is the volume of HCl solution consumed from the first titration endpoint to the second one, C_{HCl} is the concentration of HCl solution and t is the collecting time.

Results and Discussion

Flow pattern of liquid film in microchannels

To investigate the possible flow patterns of falling film in microchannels of FFMR, five liquids (deionized water, 5.2 and 12 wt % EG solutions, 50 and 110 ppm SLS solutions) have been used to perform the falling film experiments (without gas flow). Based on the images captured by high-speed CCD camera, three flow patterns were observed according to the morphology and the stability of the liquid film: “corner rivulet flow,” “falling film flow with dry patches,” and “complete falling film flow.” Figure 3 shows some representative photographs.

At low liquid flow rate, the “corner rivulet flow” pattern was observed. It was characterized by the presence of two wetted strips in the corner of microchannels and a nearly dry one in the middle bottom wall of microchannels across which little liquid bridge may be seen (Figures 3a,b). Under this flow regime, the dry strip was almost as long as the length of the microchannel and the liquid wedged in the corner of the microchannel with three-phase contact line located on the side and bottom walls.²¹

As the flow rate was increased, the flow pattern of “falling film with dry patches” was found (Figures 3c,d). In this case, there were dry patches or spots instead of dry strips present in the middle bottom wall of the microchannels. Such dry regions may be wetted again or its area increased, which may be caused by the break-up of the force balance at the upstream point of a dry patch.²² Also, three-phase contact line was observed to be not straight due to the

Table 1. Physical Properties of Liquids Used

Liquid	T^* °C	ν^\dagger (m ² s ⁻¹)	D^\ddagger ($\times 10^9$, m ² s ⁻¹)	$C^{*\S}$ (mol l ⁻¹)	Sc_L^\parallel	$\sigma^{ }$ (mN m ⁻¹)
Deionized water	25	8.97×10^{-7}	1.98	0.0324	452	72
5.2 wt % EG	25	9.40×10^{-7}	1.82	0.0319	517	69.4
12 wt % EG	25	11.04×10^{-7}	1.64	0.0310	673	67.5
30 ppm SLS	25	8.97×10^{-7}	1.98	0.0324	452	70.7
50 ppm SLS	25	8.97×10^{-7}	1.98	0.0324	452	69.8
110 ppm SLS	25	8.97×10^{-7}	1.98	0.0324	452	66.1

*Temperature.

†Kinetic viscosity.

‡Diffusivity.

§Saturated solubility.

¶Schmidt number of liquid phase.

||Surface tension.

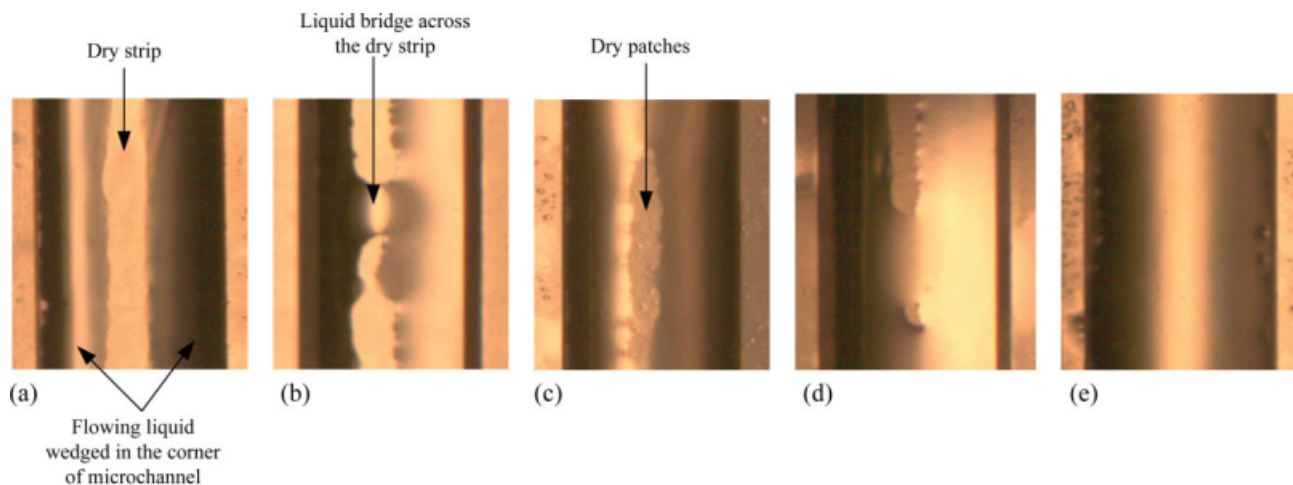


Figure 3. Flow pattern of falling film in FFMR II (microchannel cross-section: $1000\mu\text{m} \times 300\mu\text{m}$; liquid: 110 ppm SLS solution): (a, b): corner rivulet flow ($Q_L = 2\text{ ml/min}$); (c): falling film flow with dry patches ($Q_L = 3\text{ ml/min}$); (d) falling film flow with dry patches ($Q_L = 3.8\text{ ml/min}$); (e) complete falling liquid film ($Q_L = 3.9\text{ ml/min}$).

impact of surface roughness as well as heterogeneity,²³ which may further cause the undulation of the interface.

Finally when the flow rate was high enough, the bottom wall of each microchannel was covered completely by the continuous falling liquid film (Figure 3e). This flow pattern was defined here as “complete falling film flow,” which is obviously the most desirable one to perform gas–liquid absorption or chemical reaction in FFMR.

All the flow patterns were obtained without gas flow. The flow pattern in every channel was not absolutely identical under some operational conditions, so the exact transition between these flow patterns was not distinct. The relevant work is now being conducted in a single microchannel.

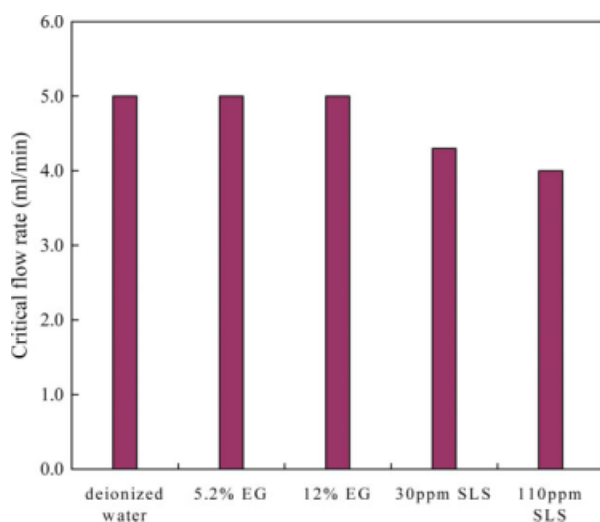


Figure 4. Critical flow rate for different kinds of liquids in FFMR II.

[Color figure can be viewed in the online issue, which is available at www.interscience.wiley.com.]

Determination of the critical flow rate

It is of considerable importance to prevent the liquid film from break-up in falling film reactors in order to ensure an efficient heat and mass transfer process.^{24–26} However, the liquid film in microchannels may not be complete by the presence of dry strips, patches, or spots, as revealed in Figures 3a–d. Therefore, there exists the minimum flow rate, namely the critical flow rate, beyond which break-up of the liquid film can be avoided. Figure 4 compares the measured critical flow rates for five liquids investigated in FFMR II. It can be seen that a reduction in the surface tension can probably lower the critical flow rate (see the results for water, 30 and 110 ppm SLS solutions shown in this figure). However, the addition of EG into water has no effect on the variation of the critical flow rate. With the increasing concentration of

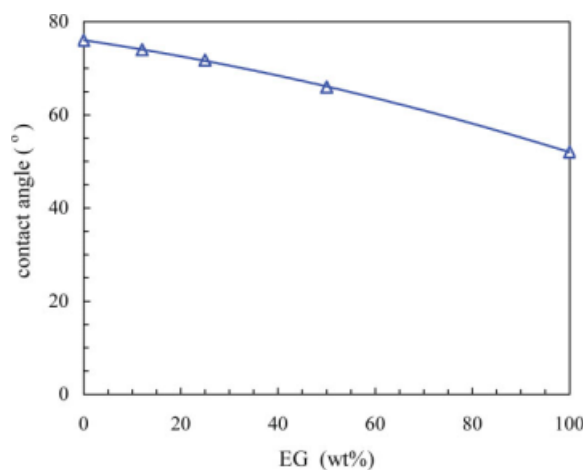


Figure 5. Contact angle of liquid used on PMMA.

[Color figure can be viewed in the online issue, which is available at www.interscience.wiley.com.]

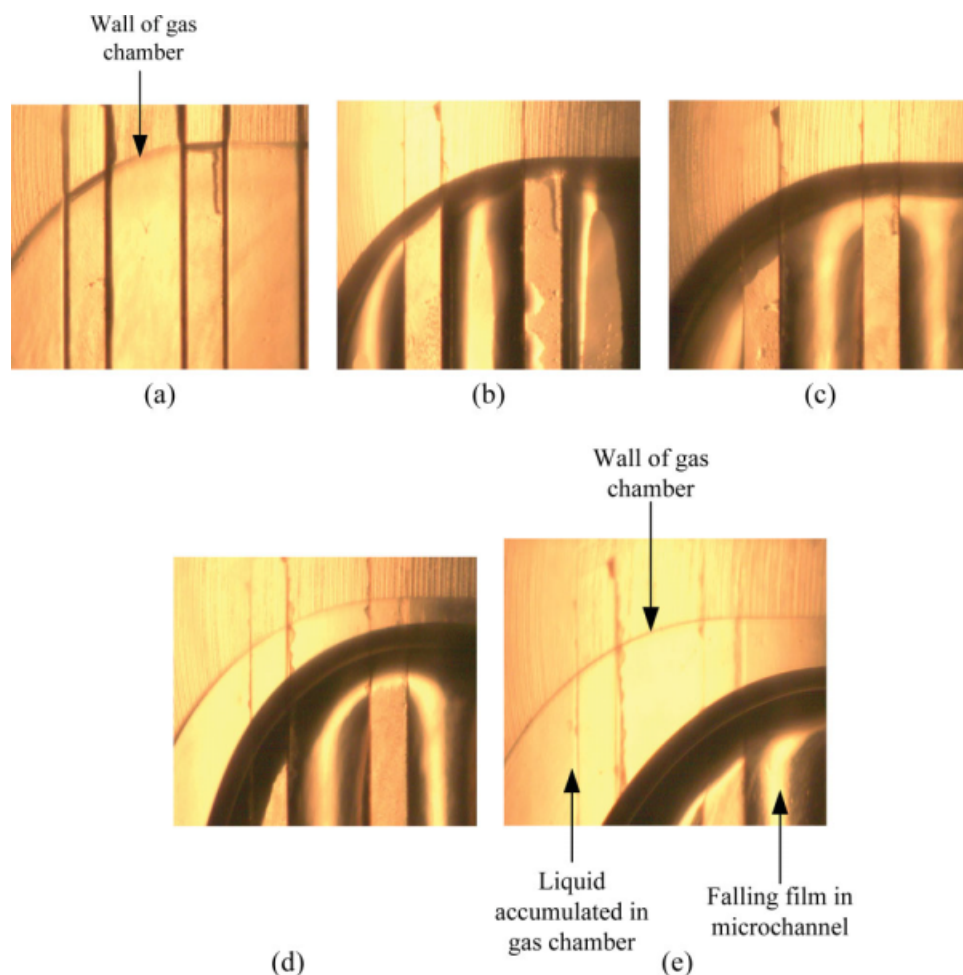


Figure 6. Image of flooding in the top part of the gas chamber of FFMR II ($d_G = 1.4$ mm) at different water flow rate (ml/min): (a) 0; (b) 2; (c) 15.5; (d) 30; (e) 50.

EG, viscosity and surface tension varied (Table 1), while the contact angles on PMMA changed little under low concentration of EG seen from Figure 5. Therefore, the critical flow rate may be caused by the complex interaction among viscosity, surface tension instead of the contact angle in this study.²⁷

Flooding phenomena

Besides liquid flowing in microchannels, a kind of flooding flow different from those in conventional falling film reactors was also observed at sufficiently high liquid flow rate. In the present FFMR, liquid from the top header flows through a very short enclosed rectangular channel (1×0.3 mm² cross section, 0.8 mm in length) to the open falling film microchannel, namely, liquid is guided from a very small space to a large one (including the open microchannels and gas chamber). Thus, liquid may expand and further wet the top wall of the gas chamber. Then, a small amount of the liquid can be introduced into the top gas chamber by the capillarity and be accumulated there. This phenomenon was named here as “jet effect.” When the amount of the liquid

accumulated in the top gas chamber was enough, the liquid would flow along the side wall of the gas chamber although the majority of liquid remained to flow in microchannels. Figures 6 and 7 show some typical images of flooding observed in FFMR II. Under these circumstances, liquid was first accumulated on the top part of the gas chamber when the flow rate was relatively lower (see Figure 6b) and then began to flow along the side wall of the gas chamber as the flow rate was increased to a certain extent (see Figure 7b). Moreover, the volume of liquid accumulated on the top part grew bigger with the increasing liquid flow rate (see Figure 6c–e). So did the amount of liquid flowing along the wall of the gas chamber (see Figure 7c,d). Meanwhile, it was also found that reducing the depth of the gas chamber also facilitated the occurrence of this flooding behavior at lower flow rates. For example, the flooding could happen at a liquid flow rate of 3 ml min^{-1} in FFMR I ($d_G = 0.8$ mm), as shown in Figure 8a. Nevertheless, the flooding could not be observed even at a flow rate of 50 ml min^{-1} in FFMR III in which d_G was increased to 3.0 mm, as can be seen from Figure 8b. This can be explained as follows: In the current design of FFMR (see Figure 1), liquid was guided to the

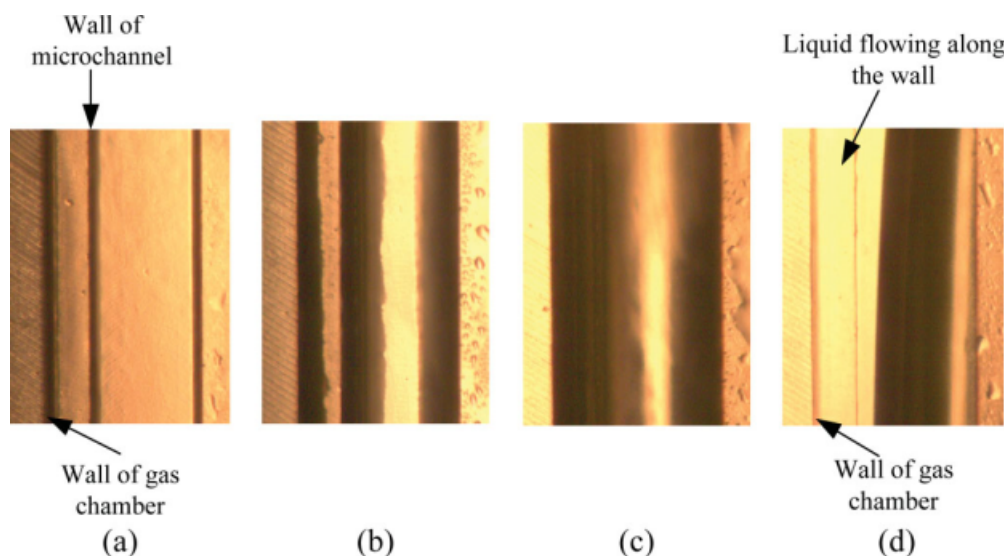


Figure 7. Image of the flooding along the wall of the gas chamber of FFMR II at different water flow rates (ml/min): (a) 0; (b) 2; (c) 15.5; (d) 50.

gas–liquid contact zone via a short enclosed microchannel section. Thus, the jet effect may make a certain part of liquid flow into the top part of the gas chamber and then to be accumulated there by capillarity. With the increasing liquid flow rate, the jet effect is more significant. Thus, more liquid will be discharged into the gas chamber. When the weight of the liquid accumulated exceeds the capillary force, the excessive liquid will flow down the side wall of the gas chamber. Moreover, as the depth of the gas chamber is further reduced, the role of capillarity will become more predominant comparing to the gravity effect, which makes the flooding to be easily initiated at much lower flow rates.

The presence of this flooding behavior is certainly disadvantageous to gas–liquid mass transfer process in FFMR by reducing the gas–liquid interfacial area and causing the entrainment of liquid by the gas flow. To avoid this, the depth of the gas chamber should be kept relatively large. However, the study of Zanfir et al.¹³ showed that the depth of the gas chamber should be reduced to lower gas-phase mass transfer resistance significantly. So there is a critical depth of the gas chamber in practical operations which can ensure both a good gas–liquid contacting and an efficient gas–liquid mass transfer process in FFMR.

Mass transfer characteristics

Mass transfer in falling film has been concerned mainly with the dependence of liquid-side mass transfer coefficient on molecular diffusivity. Several mass transfer models have been proposed to describe the absorption phenomena of gas in liquid, such as film model, surface renewal model, penetration model, film-penetration model, and eddy diffusivity theory.^{28,29} For a complete falling film flow with a flat surface profile in FFMR, Reynolds number can be defined as

$$Re_L = \frac{4\delta_L j_L}{\nu} \quad (2)$$

where δ_L and j_L denote the thickness and the mean velocity of the liquid film, respectively. According to Nusselt falling film theory, they can be expressed as:

$$\delta_L = \sqrt[3]{\frac{3Q_{LV}}{nbg}} \quad (3)$$

$$j_L = \frac{g\delta_L^2}{3\nu} \quad (4)$$

Reynolds number involved in the present study varies from 5 to 135, indicating that liquid flow was still in laminar state in the microchannel. Thus the validity of film and penetration models is examined here. According to Cussler,³⁰ Fo number is the ratio between residence time (t_L) and the diffusion time (τ_d), that is:

$$Fo = \frac{t_L}{\tau_d} = \frac{L D}{j_L \delta_L^2} \quad (5)$$



Figure 8. Image of flooding in the gas chamber in FFMRs at different water flow rates: (a) FFMR I, $d_G = 0.8$ mm, $Q_L = 3$ ml/min; (b) FFMR III, $d_G = 3.0$ mm, $Q_L = 50$ ml/min.

If $Fo \ll 1$, namely $t_L \ll \tau_d$, penetration model is applicable and mass transfer in falling film can be considered far from the equilibrium. Liquid-side mass transfer coefficient is:

$$k_L = 2\sqrt{u_{\text{surf}}D/\pi L} = 2\sqrt{1.5j_L D/\pi L} \quad (6)$$

where u_{surf} is the film surface velocity, defined as

$$u_{\text{surf}} = \frac{g\delta_L^2}{2\nu} \quad (7)$$

Otherwise if $Fo \gg 1$, film model is preferable. Liquid-side mass transfer coefficient can be expressed by the following equation:

$$k_L = D/\delta_L \quad (8)$$

CO₂ absorption experiments in the present work were all conducted under the “complete falling film flow” pattern. By performing a mass balance on an elementary shell of the falling film shown in Figure 9, the following equation can be obtained:

$$k_L(C^* - C)bdx = Q_L dC \quad (9)$$

The boundary conditions are:

$$x = 0, \quad C = 0 \quad (9a)$$

$$x = 1, \quad C = C_{\text{out}} \quad (9b)$$

Then Eq. 9 can be integrated to yield the liquid-side mass transfer coefficient as:

$$k_L = \frac{Q_L}{bL} \ln\left(\frac{C^*}{C^* - C_{\text{out}}}\right) \quad (10)$$

To examine the applicability of film and penetration models, a comparison between the measured k_L values in the experiments of CO₂ absorption into water in FFMR II and model predictions has been made, as shown in Figure 10. It can be seen that the measured k_L increases with j_L , which is consistent with the trend revealed by penetration model. On the contrary, the film model suggests a decrease of k_L with j_L . Thus it can be concluded that gas–liquid mass transfer

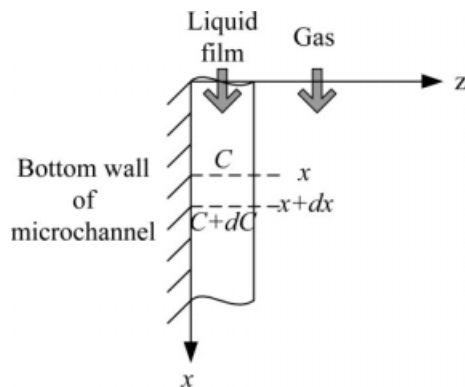


Figure 9. Elementary cell of mass transfer model.

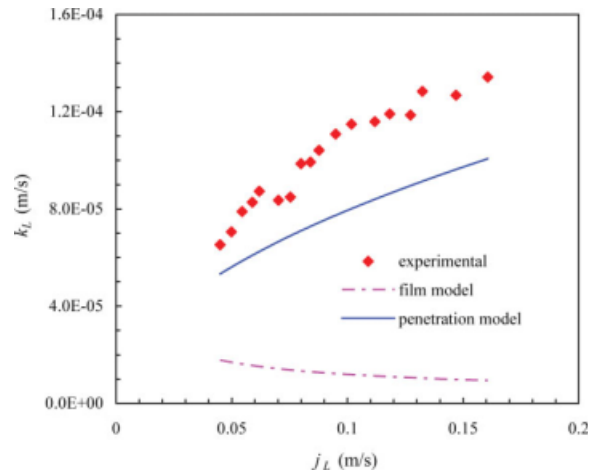


Figure 10. Comparison between measured liquid phase mass transfer coefficient with model predictions.

[Color figure can be viewed in the online issue, which is available at www.interscience.wiley.com.]

process in the present FFMRs was still far from equilibrium and penetration model held, which is also evidenced by the fact that Fo number involved in the present experiments is generally far less than 1 (ranging from 0.017 to 0.21). However, it was also noticed that the experimental data is a bit higher than the prediction of the penetration model. This deviation might be caused by the undulation of gas–liquid interface and the liquid flow pulsation from the pump used. The combined action results in an increase in the measured k_L . Another possible reason would be that Eq. 6 tends to underestimate the actual k_L in microchannels, in view of the fact that the velocity of the falling film in microchannels should be somewhat smaller than the prediction based on Nusselt theory as a result of the strong action of side-wall shear stress in microchannels.

From Figure 10, it can be also seen that the measured k_L is in the range of 5.83 to $13.4 \times 10^{-5} \text{ m s}^{-1}$. These data were obtained under the condition of $Re < 150$. For falling film in conventional reactors, it has been reported that the value of k_L is less than of $1.5 \times 10^{-5} \text{ m s}^{-1}$ in laminar flow regime.³¹ Thus, it is clear that k_L achieved in FFMR can exceed the value in conventional falling film systems by nearly one order of magnitude, implying a significant enhancement in gas–liquid mass transfer rate.

Figure 11 shows the variation of the measured k_L in FFMR II with the gas flow rate. It can be seen that a slight increase in the measured k_L was observed when there was a large increase in the gas flow rate. This indicates that strong hydrodynamic movement of liquid phase induced by the high gas flow rate such as increasing the wave region,^{32,33} may not happen in FFMR.

Effect of surface tension on k_L

In this study, aqueous solutions of 50 and 110 ppm SLS [concentrations far below the critical micelle concentration (CMC = 1900 ppm)] have been chosen as absorbent in order to make the surface tension of absorbent to change from 72

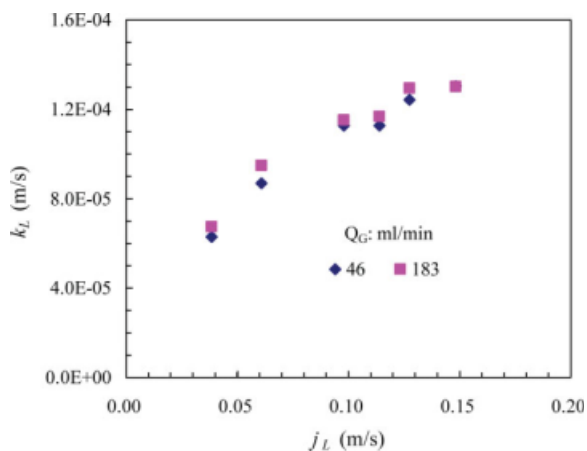


Figure 11. Effect of gas flow rate on liquid-side mass transfer coefficient.

[Color figure can be viewed in the online issue, which is available at www.interscience.wiley.com.]

to 65 mN m^{-1} . In view of the fact that the concentration of SLS was very low, the solution density and viscosity, CO_2 diffusion coefficient in the liquid can be simply assumed equal to those of deionized water. The experimental result is shown in Figure 12. It is seen that the increase in the concentration of SLS causes a slight increase in k_L at low Re_L , but its effect diminishes at high Re_L . During gas absorption into the falling film of surfactant solutions, the surface tension gradient would cause the Marangoni effect to occur,³⁴ which improves mass transfer process. Nevertheless, the addition of surfactant can also induce the barrier effect to lower mass transfer rate, the reason is that the adsorption of surfactant on gas–liquid interface may further immobilize the interface and form a resistance layer of mass transfer.^{18,35} Because the concentration of the surfactant at the interface used here is far below its critical value ($3.52 \times 10^{-5} \text{ mol m}^{-2}$),³⁶ the barrier effect was thought to be insignificant.

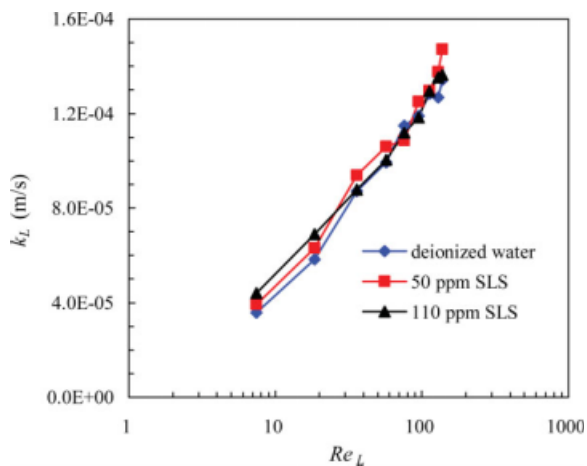


Figure 12. Effect of surface tension on liquid-side mass transfer coefficient.

[Color figure can be viewed in the online issue, which is available at www.interscience.wiley.com.]

But at low Re_L , the residence time of falling film may be longer than the time delay for the occurrence of the Marangoni convection.³⁷ Thus, it is observed that k_L increases with decreasing surface tension. At high Re_L , the residence time was so short that the occurrence of Marangoni convection might be inhibited. Thus, the variation of k_L with respect to the concentration of SLS is not obvious.

Effect of liquid viscosity on k_L

CO_2 absorption in solutions of 5.2 and 12 wt % EG solution has been studied in FFMR at the flow rate greater than 5 ml min^{-1} to avoid the break-up of falling film. From Figure 13, it seems that an increase in the concentration of EG causes a decrease in k_L . From Figure 5, addition of EG with low concentration caused very small changes in contact angles, so that the interface area can be assumed as equal (more detailed discussion is shown in the “Effect of Wettability on Mass Transfer” section). However, CO_2 diffusivity in the EG solution was less than that in water. The higher the concentration of EG, the lower the CO_2 diffusivity (Table 1). According to the above discussion, gas–liquid mass transfer process in FFMR under the present operational conditions can be approximately described by penetration model. Then as Eq. 6 suggests, k_L is dependent on CO_2 diffusivity and j_L . Therefore, it can be concluded that the decrease in the value of k_L with the increasing content of EG in water is mainly due to a significant decrease in CO_2 diffusivity. This conclusion is consistent with previous results obtained by other researchers.^{38,39} Also, the addition of EG had a negligible effect at low j_L due to the fact that CO_2 had more time to transfer across the liquid film.

Based on the mass transfer data concerning CO_2 absorption into water, 5.2 and 12 wt % EG solution, an empirical correlation can be proposed by using multivariable least squares method. That is,

$$Sh_L = 0.0145 Re_L^{0.69} Sc_L^{0.57} \quad (11)$$

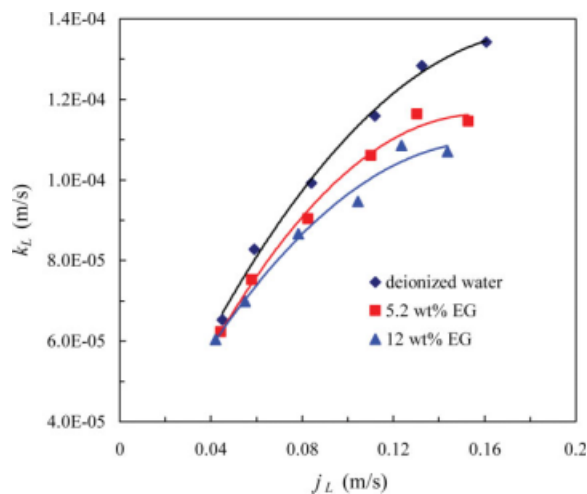


Figure 13. Effect of viscosity on liquid-side mass transfer coefficient.

[Color figure can be viewed in the online issue, which is available at www.interscience.wiley.com.]

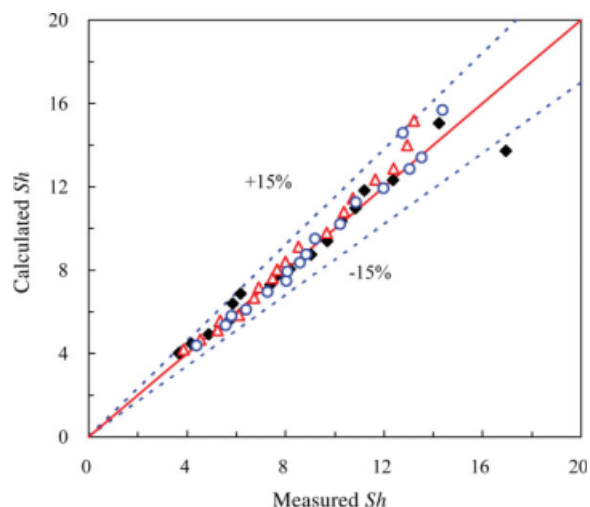


Figure 14. Comparison between measured Sh and predicted one.

[Color figure can be viewed in the online issue, which is available at www.interscience.wiley.com.]

Figure 14 shows the comparison between the measured k_L and the prediction of this correlation, where it can be seen that this correlation can describe the present experimental data fairly well.

Effect of wettability on mass transfer

The structure of gas–liquid interface is an important factor for the determination of effective interfacial area, which has an influence on the gas absorption rate. The profile of the falling film in microchannels may not be flat. As an example, Yeong et al.¹⁴ investigated the profile of the liquid film in microchannels of FFMR by using laser scanning confocal microscope and found that liquid film was a flowing meniscus under their experimental conditions. The results of Seemann et al.²¹ also revealed that the profile of liquid film in microchannels was dependent on the channel aspect ratio, liquid

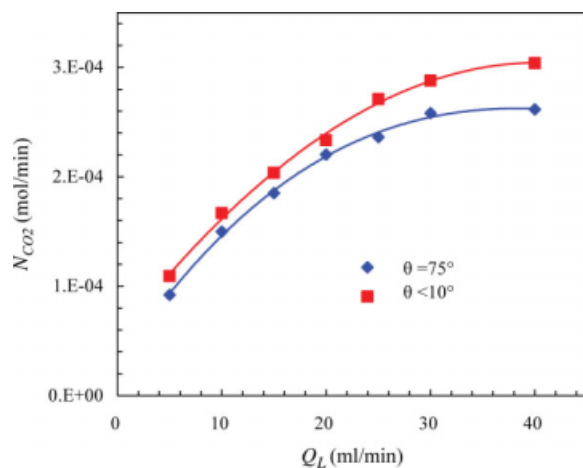


Figure 15. Effect of channel wettability on liquid side mass transfer rate.

[Color figure can be viewed in the online issue, which is available at www.interscience.wiley.com.]



Figure 16. Effect of channel wettability on the profile of falling film.

contact angle θ , and the location of three-phase contact line. Consequently, the wettability of microchannel will have a significant impact on gas–liquid mass transfer process therein.

Figure 15 compares the absorption rate of CO_2 obtained in the modified FFMR II (contact angle less than 10°) and that in the nonmodified reactor (contact angle of 75°). It can be seen that the absorption rate increases as the contact angle is reduced. In microchannels of FFMR, the profile of liquid film is usually curved (see Figure 16). As capillary number (Ca) and Weber number (We) are very small ($<10^{-3}$), the liquid film surface is supposed to be circular arcs.⁴⁰ It can be assumed reasonably that gas–liquid interfacial area is directly proportional to the length of the interface curve. The relationship between the length of the interface curve (b'), the width of microchannel (b), and contact angle (θ) can be expressed by the following equation:

$$b' = \frac{b\pi}{\cos\theta} \cdot \frac{90 - \theta}{180} \quad (12)$$

The obtained lengths of interface curve under typical contact angles are listed in Table 2. It is seen that the length of interface curve increases with the reduction of contact angle. Accordingly the interfacial area will rise. So it can be inferred that a good wettability (corresponding to lower θ) will cause an increase in mass transfer rate, as Figure 15 suggests. From Table 2 it is also clear that when the contact angle is greater than 60° , gas–liquid interface can be considered to be completely flat within an error of 5%. Therefore, the assumption of a flat interface for the deduction of k_L is reasonable.

Conclusion

Five liquids (deionized water, 5.2 and 12 wt % EG solutions, 30 and 110 ppm SLS solutions) have been used to perform the falling film experiments in FFMR. Three flow regimes were found to be “corner rivulet flow,” “falling film flow with dry patches,” and “complete falling film flow.” The third regime is the desirable one to perform gas–liquid absorption. The flooding behavior featuring in the

Table 2. Effect of Contact Angle on Surface Curve Length

Channel Width (m)	b						
θ ($^\circ$)	0	30	45	60	65	70	75
b'/b	1.57	1.21	1.11	1.05	1.03	1.02	1.01

accumulation of the liquid in the top gas chamber has been observed. As the depth of the gas chamber further decreased, the flooding was found to be initiated at much lower liquid flow rate.

CO₂ absorption in FFMR has been investigated using water, EG, and SLS solutions as absorbents under the “complete falling film flow” pattern. It was found that k_L in FFMR is in the range of 5.83 to $13.4 \times 10^{-5} \text{ m s}^{-1}$, which could be approximately estimated by penetration model. Gas flow rate was found to have negligible effect on k_L while the increase of liquid phase viscosity would yield a lower k_L . With decreasing surface tension, k_L tends to decrease as well at low Re_L but its variation is insignificant at high Re_L . Moreover, a good wettability of the microchannel wall could enhance mass transfer data significantly. Based on the obtained mass transfer data, an empirical correlation with reasonable predicting accuracy has been proposed for the prediction of k_L .

Acknowledgements

This work has been supported financially by National Natural Science Foundation of China (No. 20490208 and No. 20676129), the Ministry of Science and Technology of China (2006AA05Z233, 2007AA030206), Fund of Dalian Institute of Chemical Physics, CAS (No. K2006D62), and Open Fund of State Key Laboratory of Explosion Science and Technology, Beijing Institute of Technology (KFJJ06-1).

Notation

b = width of microchannel, m
 C = concentration, mol l^{-1}
 D = CO₂ diffusivity in liquid phase, $\text{m}^2 \text{s}^{-1}$
 d_G = depth of the gas chamber, m
 g = gravitational acceleration, m s^{-2}
 j = average velocity of falling film, m s^{-1}
 k_L = mass transfer coefficient in liquid, m s^{-1}
 L = length of microchannel, m
 n = number of microchannel
 N = absorption rate of CO₂, mol min^{-1}
 Q = flow rate, $\text{m}^3 \text{s}^{-1}$
 r = meniscus radius, m
 t = collection time, s
 t_L = liquid phase residence time, s
 u = the located velocity of liquid film, m s^{-1}
 x = the distance to the entrance of the microchannel, m
 Fr = Fourier number, $(DL/j_i \delta^2)$
 Re_L = liquid phase Reynolds number, $(4\delta_L j_i / \nu)$
 Sc_L = liquid phase Schmidt number, $\mu_L / (\rho_L D)$
 Sh_L = liquid phase Sherwood number, $k_L d_h / D$

Greek letters

δ_L = the thickness of falling film, m
 μ = liquid viscosity, Pa s
 ν = kinetic viscosity, $\text{m}^2 \text{s}^{-1}$
 τ_d = diffusion time, s
 θ = contact angle, °
 ρ = density, kg m^{-3}

Subscripts

G = gas phase
L = liquid phase
out = outlet of FFMR
surf = gas–liquid interface

Superscript

* = saturated

Literature Cited

- Dabir B, Riazi MR, Davoudirad HR. Modelling of falling film reactors. *Chem Eng Sci.* 1996;51:2553–2558.
- Talens-Alession FI. The modelling of falling film chemical reactors. *Chem Eng Sci.* 1999;54:1871–1881.
- Cao WQ, Chen GW, Li SL, Yuan Q. Methanol-steam reforming over a ZnO-Cr₂O₃/CeO₂-ZrO₂/Al₂O₃ catalyst. *Chem Eng J.* 2006;119:93–98.
- Ge H, Chen GW, Yuan Q, Li HQ. Gas phase partial oxidation of toluene over modified V₂O₅/TiO₂ catalysts in a microreactor. *Chem Eng J.* 2007;127:39–46.
- Chen GW, Li SL, Jiao FJ, Yuan Q. Catalytic dehydration of bioethanol to ethylene over TiO₂/γ-Al₂O₃ catalysts in microchannel reactors. *Catal Today* 2007;125:111–119.
- Yue J, Chen GW, Yuan Q, Luo L, Gonthier Y. Hydrodynamics and mass transfer characteristics in gas-liquid flow through a rectangular microchannel. *Chem Eng Sci.* 2007;62:2096–2108.
- Hessel V, Angeli P, Gavriilidis A, Lowe H. Gas-liquid and gas-liquid-solid microstructured reactors: contacting principles and applications. *Ind Eng Chem Res.* 2005;44:9750–9769.
- Zhao YC, Chen GW, Yuan Q. Liquid-liquid two-phase flow patterns in a rectangular microchannel. *AIChE J.* 2006;52:4052–4060.
- Jahnisch K, Baerns M, Hessel V, Ehrfeld W, Haverkamp V, Lowe H, Wille C, Guber A. Direct fluorination of toluene using elemental fluorine in gas/liquid microreactors. *J Fluorine Chem.* 2000;105:117–128.
- Hessel V, Ehrfeld W, Golbig K. Microreaction technology: industrial prospects. In: Proceedings of 3rd International Conference on Microreaction Technology, Frankfurt, 2000:526.
- Al-Rawashdeh MM, Hessel V, Löb P, Mevissen K, Schönfeld F. Pseudo 3-D simulation of a falling film microreactor based on realistic channel and film profiles. *Chem Eng Sci.* 63:5149–5159.
- Yeong KK, Gavriilidis A, Zapf R, Hessel V. Experimental studies of nitrobenzene hydrogenation in a microstructured falling film reactor. *Chem Eng Sci.* 2004;59:3491–3494.
- Zanfir M, Gavriilidis A, Wille C, Hessel V. Carbon dioxide absorption in a falling film microstructured reactor: experiments and modeling. *Ind Eng Chem Res.* 2005;44:1742–1751.
- Yeong KK, Gavriilidis A, Zapf R, Kost H J, Hessel V, Boyde A. Characterisation of liquid film in a microstructured falling film reactor using laser scanning confocal microscopy. *Exp Therm Fluid Sci.* 2006;30:463–472.
- Mikielewicz J, Moszynski JR. Minimum thickness of a liquid film flowing vertically down a solid surface. *Int J Heat Mass Transfer.* 1976;19:771–776.
- Vankayala BK, Löb P, Hessel V, Menges G, Hofmann C, Metzke D, Krtschil U, Kost HJ. Scale-up of process intensifying falling film microreactors to pilot production scale. *Int J Chem React Eng.* 2007;5:A91.
- Oyeveaar MH, Morssinkhof RWJ, Westerterp KR. Density, viscosity, solubility, and diffusivity of carbon dioxide and nitrous oxide in solutions of diethanolamine in aqueous ethylene glycol at 298 K. *J Chem Eng Data.* 1989;34:77–82.
- Sardeing R, Painmanakul P, Hebrard G. Effect of surfactants on liquid-side mass transfer coefficients in gas-liquid systems: a first step to modeling. *Chem Eng Sci.* 2006;61:6249–6260.
- Osakabe M, Hamada T, Horiki S. Water flow distribution in horizontal header contaminated with bubbles. *Int J Multiphase Flow.* 1999;25:827–840.
- Chambers RD, Fox MA, Holling D, Nakano T, Okazoe T, Sandford G. Elemental fluorine, Part 16: Versatile thin-film gas-liquid multi-channel microreactors for effective scale-out. *Lab Chip.* 2005;5:191–198.
- Seemann R, Brinkmann M, Kramer EJ, Lange FF, Lipowsky R. Wetting morphologies at microstructured surfaces. *Proc Natl Acad Sci USA.* 2005;102:1848–1852.
- Hartley D, Murgatroyd W. Criteria for the break-up of thin liquid layers flowing isothermally over solid surfaces. *Int J Heat Mass Transfer.* 1964;7:1003–1015.
- Cubaud T, Fermigier A. Advancing contact lines on chemically patterned surfaces. *J Colloid Interface Sci.* 2004;269:171–177.
- Brauner N, Moalem Maron D, Harel Z. Wettability, rewettability and breakdown of thin films of aqueous salt solutions. *Desalination.* 1985;52:295–307.

25. Paramalingam S, Winchester J, Marsh C. On the fouling of falling film evaporators due to film break-up. *Food Bioprod Process.* 2000;78:79–84.
26. Sicardi S, Baldi G, Specchia V, Mazzarino I, Gianetto A. Packing wetting in trickle bed reactors: influence of the gas flow rate. *Chem Eng Sci.* 1981;36:226–228.
27. Ruckenstein E. On the break-up of thin liquid layers flowing along a surface. *Int J Heat Mass Transfer.* 1971;14:165–169.
28. King CJ. Turbulent liquid-phase mass transfer at a free gas-liquid interface. *Ind Eng Chem Res Fundam.* 1966;5:1–8.
29. Prasher BD, Fricke AL. Mass transfer at a free gas-liquid interface in turbulent thin films. *Ind Eng Chem Process Des Dev.* 1974;13:336–340.
30. Cussler EL. *Diffusion: Mass Transfer in Fluid Systems*, 1 ed. Cambridge: Cambridge University Press, 1984: 53, 285.
31. Hameed MS, Muhammed MS. Mass transfer into liquid falling film in straight and helically coiled tubes. *Int J Heat Mass Transfer.* 2003;46:1715–1724.
32. Talens-Alession FI. The effect of superficial gas velocity on wavy films and its use in enhancing the performance of falling film reactors. *Chem Eng Technol.* 2000;23:629–632.
33. Drosos EIP, Paras SV, Karabelas AJ. Counter-current gas-liquid flow in a vertical narrow channel—liquid film characteristics and flooding phenomena. *Int J Multiphase Flow.* 2006;32:51–81.
34. Vazquez G, Antorrena G, Navaza JM. Influence of surfactant concentration and chain length on the absorption of CO₂ by aqueous surfactant solutions in the presence and absence of induced Marangoni effect. *Ind Eng Chem Res.* 2000;39:1088–1094.
35. Arzoz D, Rodriguez P, Izquierdo M. Experimental study on the adiabatic absorption of water vapor into LiBr-H₂O solutions. *Appl Therm Eng.* 2005;25:797–811.
36. Painmanakul P, Loubiere K, Hebrard G, Mietton-Peuchot M, Roustan M. Effect of surfactants on liquid-side mass transfer coefficients. *Chem Eng Sci.* 2005;60:6480–6491.
37. Hauser MJB, Oberender J, Richter S, Bartels K, Muller SC. Interfacial turbulence enhances oxygen transport into shallow liquid layers. *Physica D Nonlinear Phenomena.* 2005;205:170–180.
38. Gomez-Diaz D, Navaza JM. Effect of ethylene glycol on the CO₂/water gas-liquid mass transfer process. *Chem Eng Technol.* 2003;26:75–80.
39. Gomez-Diaz D, Navaza JM, Sanjurjo B, Vazquez-Orgeira L. Carbon dioxide absorption in glucosamine aqueous solutions. *Chem Eng J.* 2006;122:81–86.
40. Hardt S, Doffing F, Pennemann H. Simulation of hydrodynamic dispersion in gas/liquid microreactors. In: Proceedings of International Conference on Modelling and Simulation of Microsystems, Puerto Rico, 2002: 54–57.

Manuscript received July 15, 2008, and revision received Oct. 1, 2008.